Draft version September 18, 2023
Typeset using LaTeX **manuscript** style in AASTeX62

HUBS SCIENTIFIC WHITE PAPER - CLUSTER & LSS

Yiping Ao, Jiang Chang, Jian Fu, Marat Gilfanov, Liyi Gu, Hong Guo, Quan Guo, Dan Hu, Xi Kang, Weipeng Lin, Nicola Napolitano, Huanyuan Shan, Xun Shi, Aurora Simionescu, Yuanyuan Su, Jing Wang, Yu Wang, Zhonglue Wen, Fuguo Xie, Dandan Xu, Haiguang Xu, Heng Yu, Zhongsheng Yuan, Zhongxu Zhai, Congyao Zhang, Yuning Zhang, Zhongli Zhang, and Yuanyuan Zhao

1. GALAXY CLUSTERS AND LARGE-SCALE STRUCTURE

Structures in the Universe have formed bottom-up as dark matter and baryonic matter aggregate over cosmic time via hierarchical gravitational collapse and eventually develop into the Large-Scale Structure (LSS), including knots, filaments, walls, and voids. While the dynamics of LSS is dominated by dark matter whose assembly and evolution can be well described by gravitational effects, the formation and evolution of baryonic structures are strongly affected by ineligible astrophysical processes. Galaxy clusters, the end product of hierarchical structure formation, are mostly located at knots of the LSS and are the largest virialzed systems in the Universe.

Since the early 20^{th} century, galaxy clusters and groups have been among the most interesting subjects in astrophysical and cosmological studies. A typical galaxy cluster contains hundreds to thousands of member galaxies, with a total mass of 10^{14-15} $M_\odot$ and a size of a few Mpc. The galaxy groups, on the other hand, can be deemed as miniature versions of galaxy clusters, containing a few to tens of member galaxies. The composition of galaxy clusters is dominated by dark matter (about $\sim 80\%$) (Diaferio et al. 2008), which cannot be directly observed but can be studied through the observations of baryonic matter. Within the baryonic matter of a typical cluster, $\sim 70-90\%$ is the hot and diffuse X-ray emitting plasma known as the Intra-Cluster Medium (ICM) in the case of galaxy clusters, or Intra-Group Medium (IGrM) in the case of galaxy groups (both referred to as "clusters" and "ICM" in this chapter unless otherwise specified), and gas mass is on average ten

times larger than the mass in stars, ranging from $M_*/M_g \approx 0.2$ to ≈ 0.05 (Kravtsov & Borgani 2012). Therefore, understanding the thermal, dynamical, and chemical properties of the ICM via X-ray observations is essential and valuable to probe the formation and evolution of galaxy clusters and further those of the Universe.

In the past two decades, new generation X-ray satellites such as *Chandra*, *XMM-Newton*, *Suzaku* have greatly enhanced our understanding of the baryon distribution, the gas dynamics, and the chemical history of galaxy clusters. However, limited by instrumental capabilities, there are still crucial problems left to be solved, i.e., the status and physics of multi-phase gas, the impact of mergers and AGN feedback on ICM evolution, and a complete picture of the chemical enrichment history of galaxy clusters. The *HUBS* mission designed to observe in a softer X-ray band with superb energy resolution, wide field-of-view (FoV), and sufficient angular resolution is expected to provide new insights into these areas of interest.

1.1. *Undetected Baryons in the Universe*

In the past decades, our knowledge of the Universe has advanced rapidly through the observations of the cosmic microwave background (CMB), Type Ia supernovae (SNIa), and the large-scale structure of galaxy distribution, which all served to fortify the ΛCDM cosmological model and provide constraints on the matter and energy distributions. The latest results from Planck Collaboration et al. (2020) indicate that the Universe is comprised of 68% of dark energy, 26% of cold dark matter, and 5% of baryonic matter under within the frame of the ΛCDM model. However, although taking up only a small percentage of the Universe, the baryons are responsible for all the observable electromagnetic signals in astronomical observations. On the other hand, the distribution and state of baryons in the Universe are tightly related to the formation and evolution of the Universe and the corresponding astrophysical processes. With the collapse of initial perturbations, the distribution of dark matter evolved to form the cosmic web structure, including knots, filaments, walls, and voids. In the meantime, the baryonic matter follows dark matter halos, hierarchically forming stars, galaxies, and galaxy clusters.

Through observations of the present-day Universe, a deficit of detected baryons relative to the predicted density synthesized in the Big Bang was noted (Cen & Ostriker 1999). Current theories indicate that the rest of the baryonic matter should be found in the Warm-Hot Intergalactic Medium (WHIM) in the circumgalactic and intergalactic space (CGM and IGM). The location and physical state of the undetected baryons are intertwined with critical questions in astronomy, such as star formation and stellar feedback, galaxy formation and evolution, AGN feedback, and the co-evolution of black holes and galaxies. Understanding the undetected baryons can provide evidence and constraints for current cosmological models. It is thus crucial to understand how non-linear processes such as heating due to gravitational collapse, cooling, star formation, and AGN activities affect baryons' distribution and physical state.

Cosmological hydrodynamical simulation is a powerful tool to predict the distribution of baryonic gas and guide observations by numerically solving for the non-linear evolution of matter. Since the 2000s, the cosmological hydrodynamical simulation approach with baryonic processes included has gradually taken over pure dark matter simulations to become the main method for cosmological simulations via the incorporation of astrophysical equations such as shocks, turbulence, ionization, radiative cooling, star formation, supernova feedback, black hole accretion and feedback, as well as radiative transfer, magnetic fields, and cosmic rays (Naab & Ostriker 2017). Gaseous baryons can be classified into cold gas ($< 10^4$ K), cool gas ($10^4 - 10^5$ K), warm-hot gas ($10^5 - 5 * 10^6$ K), and hot gas ($> 5 * 10^6$ K). Simulations have found that the missing baryons could be found in warm-hot intergalactic medium near the outskirts of galaxies, especially on the nodes of the cosmic web filaments (Cen & Ostriker 1999; Davé et al. 2001; Vogelsberger et al. 2014; Schaye et al. 2015). High-precision simulations can also predict the distribution of WHIM around individual galaxies. For example, the NIHAO project (Wang et al. 2015, 2017) found that 35% of baryons are "lost" in the outskirts of galaxies beyond their virial radius. Fig. 1 shows an example of the distribution of gas in different phases.

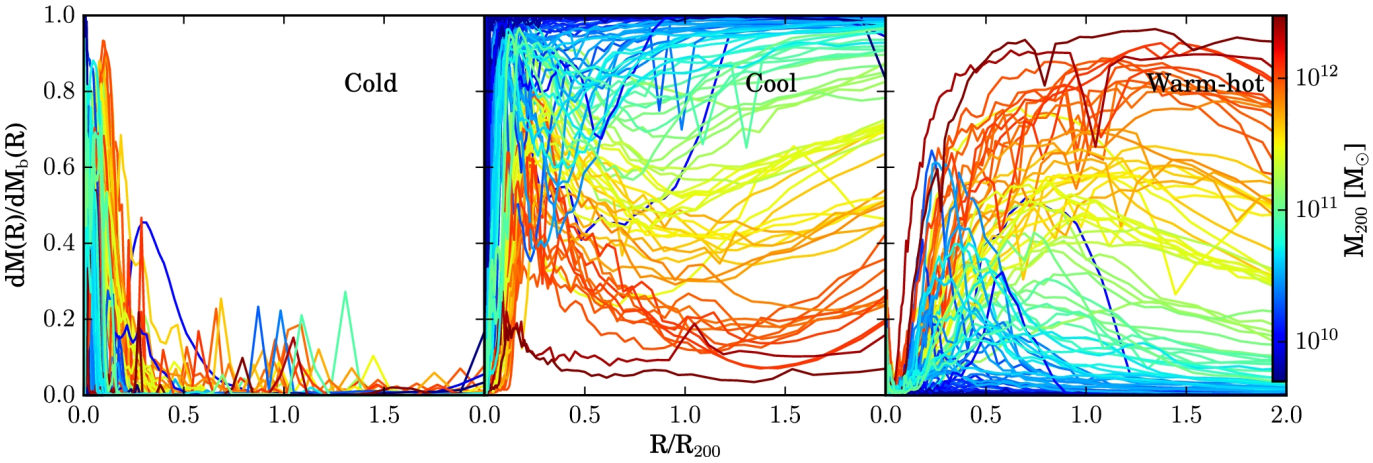

Figure 1. Radial profile of mass fraction of cold, cool, and warm-hot gas to the total baryonic mass at $z = 0$ of the simulated NIHAO sample (Wang et al. 2017)

To further resolve the uncertainties in current hydrodynamical simulations, observations of WHIM in the soft X-ray band are required. Combined with simulations, *HUBS* is expected to improve understanding in the following areas:

- X-ray imaging spectroscopy in synergy with multi-wavelength observations of the SZ effect and 21 cm signal
- Contribution from feedback processes to WHIM distribution
- The distribution of baryonic matter in the cosmic web

1.2. *Warm and Hot Baryons in the Galaxy Clusters*

The vast space between member galaxies in galaxy clusters is filled with ICM, diffuse and hot gas ionized due to shock heating by the release of gravitational energy and accretion during cluster formation. The typical temperature for the ICM is $10^7 - 10^8$ K, meaning its dominant radiation mechanism is X-ray emission due to bremsstrahlung emission and line emission of heavy elements. The typical electron density of the ICM is $10^{-4} - 10^{-2}$ cm^3, decreasing rapidly with increasing radius as $\sim r^{-3}$ and even more cuspily beyond r_{500} Patej & Loeb (2015).

Even though current models can well describe the global properties of ICM for the most part, non-gravitational effects in the cluster core area and deviation from hydrostatic equilibrium in the

outskirts bring high complexity and can only be studied in detail with future X-ray instruments with better resolution and sensitivity.

1.2.1. *Cooling Flow and Heating Mechanisms*

About one-third to half of the nearby galaxy clusters host cool cores (Rossetti & Molendi 2010; Andrade-Santos et al. 2017), which typically appear as a central surface brightness enhancement with steeply decreased temperature and increased gas density. As the cool-core clusters experience significant radiative cooling in the center, a substantial amount of inward gas flow and extreme star formation are expected (Fabian 1994). Although cold molecular gas (Russell et al. 2019; Olivares et al. 2019) and warm molecular and atomic gas (Liu et al. 2020) have been detected, which could be cooled from the hot ICM, there had been little evidence for the predicted portion of cooling flow even with the launch of *Chandra* and *XMM-Newton* (i.e., the "cooling flow problem";McDonald et al. (2018) and references therein), implying that some additional heating mechanism is required to balance the cooling.

The central radio AGN is the current consensus for the primary energy source to prevent massive gas cooling and star formation. They operate in radio mode and drive powerful jets that inflate bubbles filled with relativistic particles to up to 200 kpcs in the ICM, and transport energy through mixing, shocks, sound waves, and cosmic ray streaming (Hlavacek-Larrondo et al. (2022) and references therein). The power implied from X-ray cavities carved out by AGN jets match the cooling luminosity (Churazov et al. 2002; Bîrzan et al. 2004), indicating the AGN feedback can be sufficient to balance the cooling. However, without the observation of cool ICM, little is understood about how such a tight balance is achieved, especially for the low-mass systems whose AGN activities are less powerful, whereas a similar entropy profile was observed as the high-mass systems (Panagoulia et al. 2014; Babyk et al. 2018).

To solve the gas cooling problem, it is essential to resolve the ICM into multi-phase components with an emphasis on the low-temperature end, which requires future instruments to cover the $<$ 1.5 keV energy band with eV scale energy resolution to diagnose the spectral lines of metals at

different ionization states. *HUBS*, with its designated energy band for soft X-ray and superior energy resolution, is expected to accomplish the following:

- Search for bulk quantities of cool gas (0.1 – 1.5 keV) near the BCG with accurate measurement of gas temperature, metal abundance, and density through high precision spectral line diagnostics (especially O_{VII}, O_{VIII}, Ne_{IX}, and Ne_{X}, etc.)
- Provide observational evidence of AGN heating by quantifying the amount and velocity of jet-driven outflows
- Solve for the spatial and temporal balance between radiative cooling and AGN heating

1.2.2. *Outskirts of Galaxy Clusters*

As the largest virialized systems, galaxy clusters are formed at the nodes of the large-scale structure and continue to accrete matter from the cosmic filaments. The outskirts of galaxy clusters, usually subjectively defined as outside of r_{500} and within the virial radius, occupy about 90% of the cluster volume, and are expected to undergo energetic activity as material is accreted into the dark matter halo's potential (Reiprich et al. 2013).

Deviation from equilibrium states and gas clumping due to structure formation effects in this region may induce a bias when performing analysis under equilibrium assumptions. The apparent baryon fraction in the outskirts was found to be higher than the cosmic mean value for the Perseus Cluster (Simionescu et al. 2011) and Virgo Cluster (Simionescu et al. 2017) using *Suzaku* data, suggesting clumpy distribution of gas. Compared with relaxed systems, post-merger and merger systems show gas clumping of a higher extent and closer to the cluster cores appear in post-merger and merger systems as opposed to relaxed systems (Eckert et al. 2013; Vazza et al. 2013). Nevertheless, there is still a considerable amount of clumping outside r_{500} for relaxed systems (Zhu et al. 2021). Therefore, studying gas clumping can help understand bias in cluster gas and total mass, as well as entropy measurements, and provide details of structure formation in the ICM.

Further out beyond the virial radius, observations of Abell 2744 indicated hot filamentary structures coincident with over-densities of galaxies and dark matter shown in Fig. 2. These filaments comprise

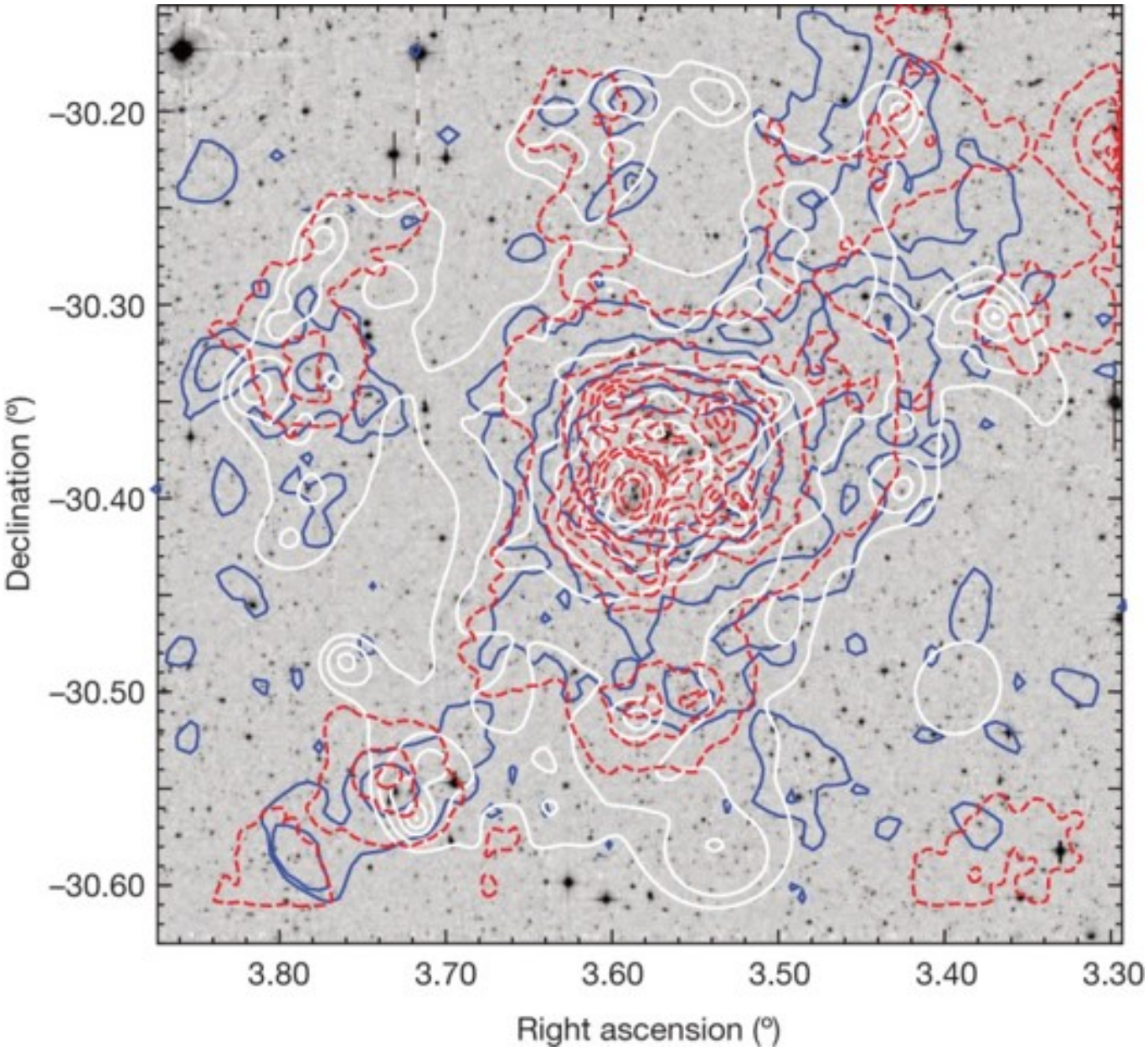

Figure 2. CFHT image of Abell 2744 and the surrounding LSS. The contours show X-ray isophotes (blue), mass distribution reconstructed from combined strong and weak lensing (white), and optical light (dashed red) Eckert et al. (2015).

5-10% of baryonic gas (Eckert et al. 2015), indicating that a large fraction of the undetected baryons resides in filaments of the LSS.

Deep X-ray observations of the cluster outskirts can deepen our understanding of the formation and accretion process of galaxy clusters. Unfortunately, as the X-ray surface brightness drops roughly as

the square of gas density, the signal-to-noise ratio in galaxy cluster outskirts obtained from current X-ray missions is insufficient due to their high and sometimes unstable particle background. Since *HUBS* is designed to operate in a near-Earth orbit, which is expected to receive an order of magnitude lower solar particles than the telescopes in high elliptical orbits, it is expected to be an ideal instrument for probing the outskirts of galaxy clusters.

1.3. *Cluster Dynamics*

As mentioned in section 1.2.1, some heating mechanism must exist to preclude gas from cooling in the cluster core, with AGN activity being the most probable source (Fabian 2012). However, it is still unclear how this heating energy is transferred to the ICM. Zhuravleva et al. (2014) and Hitomi results indicated turbulence as a probable energy transfer channel. The energy to heat ICM is first released through the kinetic energy of the turbulence, then gradually dissipated to smaller scales and eventually converted to heat. Further observational constraints on cluster dynamics can enhance knowledge of non-thermal processes and help model the thermodynamics of the ICM.

1.3.1. *Particle Acceleration in the ICM*

In addition to thermal processes, non-thermal processes are also crucial in the ICM. Since the 1950s, there have been many detections of synchrotron emission and inverse Compton scattering in the ICM due to relativistic electrons. Both observations and simulations indicate that diffuse radio emission exists in over a third of galaxy clusters. The diffuse emission spans a range from a few hundred kpcs to Mpc scale in different forms, often classified as radio halos, mini halos, and radio relics (Feretti et al. 2012). Radio bridges were also discovered at the early stage of cluster mergers (Govoni et al. 2019; Botteon et al. 2020). Our current knowledge for the formation of these radio sources are: (1) early AGN, star-forming activity, and other unknown processes contribute significant quantities of fossil relativistic electrons; (2) fossil relativistic electrons get re-accelerated through the Fermi-II process due to Mpc-scale turbulence produced in galaxy cluster mergers to form radio halos; (3) merger-induced low-Mach number shocks rearrange the magnetic field, causing fossil electrons and high-energy electrons to travel back and forth through the shocks and get re-accelerated through

the Fermi-I process to form radio relics (Brunetti & Jones 2014); (4) Oscillations of gas in the cluster core region due to minor mergers or central AGN activities accelerate the fossil relativistic electrons and produce mini halos within a few hundred kpcs of the cluster core.

While major mergers can be identified with radio relics on the periphery of galaxy clusters, minor mergers are sometimes difficult to be distinguished from AGN effects with current capabilities. For example, the compact group HCG62 exhibits a surface brightness excess at about 36 kpc from the core, which may correspond to either shock heating due to AGN jets (Gitti et al. 2010) or gas sloshing in a merger event (Rafferty et al. 2006). Hu et al. (2019) found through hydrodynamical simulations that a major merger (mass ratio 3:1) can be solely responsible for the structure, but the effects of AGN still cannot be ruled out.

With the large FoV and superior energy resolution of HUBS, it will be possible to provide a complete picture of gas dynamics in nearby galaxy clusters, thus giving insights into the evolution of the galaxy clusters in combination with metallicity distribution measurement (to be addressed in section 1.4). The following aspects could be addressed with *HUBS*:

- Model the energy transport due to turbulence by measuring the velocity field of the ICM
- Constrain the intensity and distribution of magnetic fields in galaxy clusters
- Furthermore, improve understanding of particle acceleration mechanisms with X-ray observations to help understand the formation and evolution of diffuse radio sources in synergy with radio observations (i.e., LOFAR, MWA, SKA).

1.3.2. *Observation of non-thermal electrons*

Observationally, the non-thermal cosmic ray electrons (CRe) exhibit the following features in galaxy clusters: (1) the CRe's characteristic continuum emission is most prominent in hard X-ray and gamma-ray bands; (2) CRe can disrupt the ionization equilibrium of the ICM spectrum by ionizing the ICM; and (3) interactions between CRe and hot ICM can result in changed line ratios due to resonance effects. While (1) cannot be observed with soft X-ray instruments, (2) and (3) can significantly impact ICM observations. Gu et al. (2018) showed that using line ratios of characteristic

lines and other major lines (i.e., H_α), CRe can be quantitatively measured, which can be achieved with *HUBS*' good energy resolution and sensitivity, and therefore provide insights into the origin of fossil relativistic electrons in the diffuse radio sources.

1.4. *Chemical History of Galaxy Clusters*

Heavy elements (elements heavier than helium), or metals, in the Universe are primarily formed through thermonuclear processes in different stages of a star's lifetime, in the core of stars, or during supernova explosions. Core-collapse supernovae (SNcc) explosions at the end-of-life of massive stars ($\gtrsim 10M_\odot$) eject mainly oxygen (O), neon (Ne), magnesium (Mg), silicon (Si), and sulfur (S); type Ia supernovae (SNIa) explosions of white dwarfs (WD) at the end-of-life of low-mass stars ($\lesssim 10M_\odot$) release large amounts of argon (Ar), calcium (Ca), chromium (Cr), manganese (Mn), iron (Fe), and nickel (Ni) as well as Si and S; during asymptotic giant branch (AGB) phase of low-mass stars, lighter elements such as carbon (C) and nitrogen (N) are released via galactic winds (Schindler & Diaferio 2008).

When studying the chemical composition in the astrophysical context, metal abundance, or metallicity (Z) is used to describe the content of a certain element. The abundance of an element is defined as the fraction of atoms of that element over hydrogen atoms with respect to that fraction of the sun ($Z_\odot$). Because the diffuse ICM is in collisional ionization equilibrium (CIE), its abundance of heaving elements can be determined by emission lines over the bremsstrahlung continuum.

Mitchell et al. (1976) first detected Fe-K line emission in the ICM of the Perseus Cluster. Since then, observations have revealed that metals are not constrained to where they were formed, but exist throughout the vast ICM on Mpc scales. In order to answer questions such as when, where, and how the ICM got chemically enriched with metals, it is essential first to map out the spatial distribution of heavy elements. Current observations of nearby clusters have shown that (see Mernier et al. (2018); Mernier & Biffi (2022) for detailed reviews):

- The abundance ratios in the ICM are consistent with radius and remain very similar to that of the Milky Way (de Plaa et al. 2017; Hitomi Collaboration et al. 2017; Simionescu et al. 2019)

- In cool-core clusters, metal abundance (both SNIa and SNcc products) tends to be centrally peaked, while non-cool-core clusters have flatter central profiles (Mernier et al. 2017; Lovisari & Reiprich 2019)
- Metal abundance converges to $\sim 0.3 Z_{\odot}$ towards the outskirts of galaxy clusters (Urban et al. 2017; Simionescu et al. 2017)
- High metallicity substructures exist and show a correlation with X-ray cavities and/or cold fronts (Kirkpatrick & McNamara 2015; Sanders et al. 2016; Hu et al. 2019)

The observational evidence above supports the *early enrichment scenario*, where the bulk of the metals was released from galaxies and mixed into the ICM before cluster assembly ($z \sim 2-3$): the observed homogeneity of abundance in the cluster outskirts is a result of accretion of pre-enriched gas during cluster formation, and the central metal peak was formed either in-situ during early BCG assembly or via infall of already enriched gas. As shown in Fig. 3, this scenario also agrees with cosmological hydrodynamical simulations (e.g., Rasia et al. (2015); Biffi et al. (2018)). Apart from the global uniformity, local metallicity structures are also indications of metal redistribution, which traces gas motions due to AGN jets, ram-pressure stripping, gas sloshing, and cluster mergers.

Even though the overall picture of early enrichment seems clear, the current observations are still facing ineligible instrumental limitations, e.g., poor energy resolution - compromising the ability to differentiate individual spectral lines, rapid decay of effective area towards low energy - imposing difficulty in separating multi-phase components, and small FoV - making it impossible to analyze outskirts of nearby systems in detail without multiple deep pointings, etc. Fortunately, the limitations above are all expected to be addressed with *HUBS* with its $\sim$ eV level resolution, 500 cm^2 effective area at 0.5 keV, and 1 deg x 1 deg FoV, which would capture Abell 1795, as an example, to its r_{200} with one deep pointing.

1.5. *Cosmology with Galaxy Clusters*

In Cold Dark Matter (CDM) models, galaxy clusters are formed from the collapse of initial perturbations of a typical comoving scale of about 10 h^{-1}Mpc[1], over which gravitational dynamics in

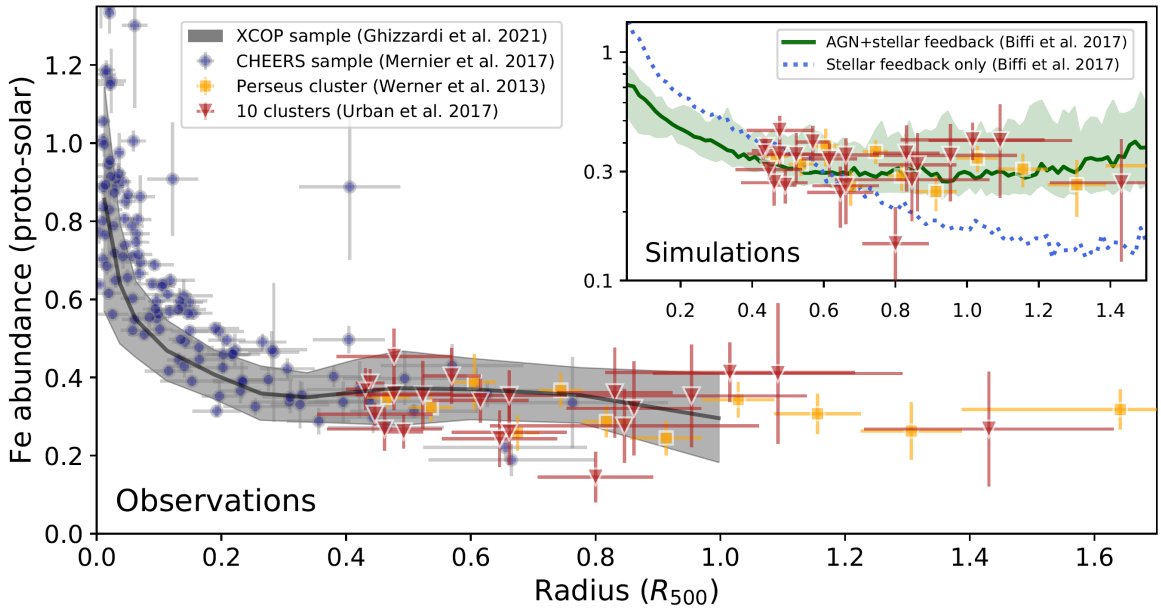

Figure 3. Fe abundance profiles in cool-core clusters in observations and simulations Mernier & Biffi (2022).

the linear or weakly non-linear regime dominate, making it relatively simple to describe structure formation, and below which the complex astrophysical processes become ineligible in the evolution of baryonic structures. Therefore, galaxy clusters are at a very special place in cosmology and have been studied as one of the powerful tools for placing constraints on cosmological parameters (See Borgani (2008) and Allen et al. (2011) for extensive reviews).

1.5.1. *Cluster Population*

The most prominent approach among current methods for cosmology with galaxy clusters is using the observed cluster population to constrain the formation and evolution of dark matter halos. The halo mass function (HMF), defined as the number density of virialized halos found as a function of mass and redshift, in some assumed cosmology, can be theoretically estimated by the PS theory (Press & Schechter 1974), and calibrated by numerical N-body dark matter simulations (Jenkins et al. 2001; Springel et al. 2005; Tinker et al. 2008; Watson et al. 2013) or cosmological hydrodynamical simulations incorporated (Cui et al. 2012; Cusworth et al. 2014; Bocquet et al. 2016; Castro et al. 2021). Based on the HMF deduced from observables of a cluster sample through scaling relations, combined with distance measurements, essential parameters of the cosmological model such as the

matter density $\Omega_{\rm M}$, the amplitude of linear density fluctuation σ_8, dark energy equation of state w, and the Hubble constant H_0 can be inferred. Large cluster samples have been collected with wide-field surveys through the SZ effect (e.g., Planck Collaboration et al. (2016); Bleem et al. (2020); Hilton et al. (2021)), weak lensing (e.g., Miyazaki et al. (2018); Oguri et al. (2021)), and X-ray (e.g.m Vikhlinin et al. (2009); Adami et al. (2018); Liu et al. (2022)) surveys.

Recent results from *eROSITA* Final Equatorial Depth Survey (eFEDS) containing 455 clusters within the redshift range of $0.1 < z < 1.2$, in combination with the Hyper Suprime-Cam (HSC) survey data for mass calibration, demonstrated capability to constrain $\Omega_{\rm M}$, σ_8, and w in a flat ΛCDM cosmology to comparable levels as independent methods such as those adopted by Planck CMB (Planck Collaboration et al. 2020), the Dark Energy Survey (DES) (Abbott et al. 2022), and the SPT-SZ survey (Bocquet et al. 2019).

The accuracy of completeness of the cluster sample in both mass and redshift, crucial for putting powerful constraints on cosmological parameters, requires deep and extensive surveys, which can be time-consuming. As a result, current cluster samples suffer from a deficiency in both relatively high-z and the low-mass end (current cluster population comprehensively investigated only until $z \sim 0.1-0.2$ and $M > 10^{14} M_{\odot}$. The complete *eROSITA* All-Sky Survey (eRASS) is expected to detect $\sim 10^5$ clusters Pillepich et al. (2018), making it the most promising upcoming cosmology results. However, the shallow exposure time of 2.5 ks per field would limit its ability to detect low-mass, high redshift clusters (i.e., $< 10^{14} M_{\odot}$ and > 0.2). *HUBS*'s low instrumental background and high resolving power will allow it to resolve faint galaxy clusters and groups among foreground/background point sources in narrow-band images (vicinity of $O_{\rm VII}$ and $O_{\rm VIII}$ lines) (Zhang et al. 2022). Fig. 4 shows the early prediction of cosmological constraints using cluster detection limit of *HUBS* compared with other cosmological constraints.

1.5.2. *Cluster Gas Mass Fraction*

Another method to constrain cosmological models with galaxy clusters is using the gas mass fraction (f_{gas}), where the completeness of the cluster sample in terms of mass is not essential. Using X-ray observations alone or combined with SZ effect observations, f_{gas} of a sample of bright and dynamically

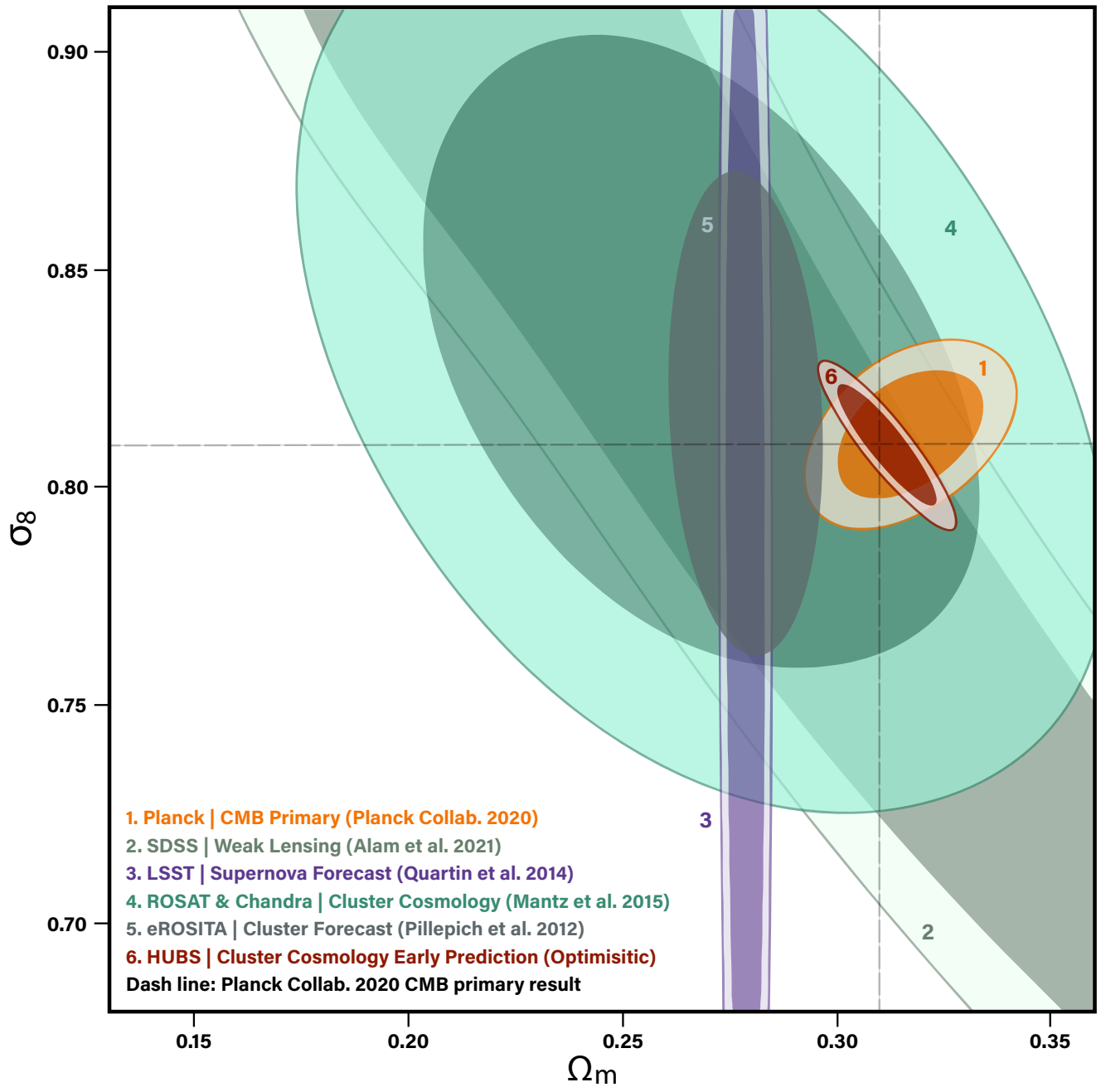

Figure 4. Forecast of cosmological constraints of $\Omega_{\rm M}$ and σ_8 by HUBS, comparing to results from *Planck* CMB study, SDSS weak lensing study, LSST supernova forecast, *ROSAT* and *Chandra* cluster survey, and *eROSITA* cluster forecast (references in the picture). The *eROSITA* cluster forecast marks the 1σ distribution of the parameter space. (cite Science China paper)

relaxed clusters can be robustly determined, which can well constrain the matter density parameter $\Omega_{\rm M}$. Additionally, once f_{gas} measured from X-ray data within a given angular aperture is related to its angular diameter as $\sim {d_{\rm ang}}^{3/2}$, the redshift dependence of f_{gas} can provide constraints for the dark matter density Ω_Λ and/or its equation of state w, depending on the choice of the cosmological model. This method has shown consistent results with CMB, SNIa, and BAO measurements (Allen et al. 2008; Mantz et al. 2022).

Although the f_{gas} measurements can be made at radii of any over-density, choosing an aperture with minimum scatter would provide better cosmological constraints. In the cluster core, non-gravitational processes, especially feedback from AGN, can contribute to ICM entropy out to $\sim \ 0.35r_{200}$ (Zhu et al. 2021). In the outskirts, accretion-induced gas clumping becomes significant (refer to section 1.2.2), and the X-ray background of current instruments brings additional uncertainties. Most of the current works generally use only a ring around r_{2500} due to the rapidly reduced signal-to-noise ratio further out. Even though simulation from Borgani & Kravtsov (2011) shows acceptable scatter in the $\sim r_{2500}$ region, it can be improved if the aperture is extended to r_{500}.

The large FoV of *HUBS* would bring a considerable advantage over current instruments by allowing for $r_{500} - r_{200}$ coverage with an improved signal-to-noise ratio of more nearby clusters, which is infeasible in current works on gas fraction studies. Furthermore, its superior spectral resolution can provide an accurate measurement of gas motions to better identify if clusters are relaxed during sample selection.

REFERENCES

Abbott, T. M. C., Aguena, M., Alarcon, A., et al. 2022, PhRvD, 105, 023520

Adami, C., Giles, P., Koulouridis, E., et al. 2018, A&A, 620, A5

Allen, S. W., Evrard, A. E., & Mantz, A. B. 2011, ARA&A, 49, 409

Allen, S. W., Rapetti, D. A., Schmidt, R. W., et al. 2008, MNRAS, 383, 879

Andrade-Santos, F., Jones, C., Forman, W. R., et al. 2017, ApJ, 843, 76

Babyk, I. V., McNamara, B. R., Nulsen, P. E. J., et al. 2018, ApJ, 862, 39

Biffi, V., Mernier, F., & Medvedev, P. 2018, SSRv, 214, 123

Bîrzan, L., Rafferty, D. A., McNamara, B. R., Wise, M. W., & Nulsen, P. E. J. 2004, ApJ, 607, 800

Bleem, L. E., Bocquet, S., Stalder, B., et al. 2020, ApJS, 247, 25

Bocquet, S., Saro, A., Dolag, K., & Mohr, J. J. 2016, MNRAS, 456, 2361

Bocquet, S., Dietrich, J. P., Schrabback, T., et al. 2019, ApJ, 878, 55

Borgani, S. 2008, in A Pan-Chromatic View of Clusters of Galaxies and the Large-Scale Structure, ed. M. Plionis, O. López-Cruz, & D. Hughes, Vol. 740, 24

Borgani, S., & Kravtsov, A. 2011, Advanced Science Letters, 4, 204

Botteon, A., van Weeren, R. J., Brunetti, G., et al. 2020, MNRAS, 499, L11

Brunetti, G., & Jones, T. W. 2014, International Journal of Modern Physics D, 23, 1430007

Castro, T., Borgani, S., Dolag, K., et al. 2021, MNRAS, 500, 2316

Cen, R., & Ostriker, J. P. 1999, ApJ, 514, 1

Churazov, E., Sunyaev, R., Forman, W., & Böhringer, H. 2002, MNRAS, 332, 729

Cui, W., Borgani, S., Dolag, K., Murante, G., & Tornatore, L. 2012, MNRAS, 423, 2279

Cusworth, S. J., Kay, S. T., Battye, R. A., & Thomas, P. A. 2014, MNRAS, 439, 2485

Davé, R., Cen, R., Ostriker, J. P., et al. 2001, ApJ, 552, 473

de Plaa, J., Kaastra, J. S., Werner, N., et al. 2017, A&A, 607, A98

Diaferio, A., Schindler, S., & Dolag, K. 2008, SSRv, 134, 7

Eckert, D., Molendi, S., Vazza, F., Ettori, S., & Paltani, S. 2013, A&A, 551, A22

Eckert, D., Jauzac, M., Shan, H., et al. 2015, Nature, 528, 105

Fabian, A. C. 1994, ARA&A, 32, 277

—. 2012, ARA&A, 50, 455

Feretti, L., Giovannini, G., Govoni, F., & Murgia, M. 2012, A&A Rv, 20, 54

Gitti, M., O'Sullivan, E., Giacintucci, S., et al. 2010, ApJ, 714, 758

Govoni, F., Orrù, E., Bonafede, A., et al. 2019, Science, 364, 981

Gu, L., Zhuravleva, I., Churazov, E., et al. 2018, SSRv, 214, 108

Hilton, M., Sifón, C., Naess, S., et al. 2021, ApJS, 253, 3

Hitomi Collaboration, Aharonian, F., Akamatsu, H., et al. 2017, Nature, 551, 478

Hlavacek-Larrondo, J., Li, Y., & Churazov, E. 2022, arXiv e-prints, arXiv:2206.00098

Hu, D., Xu, H., Kang, X., et al. 2019, ApJ, 870, 61

Jenkins, A., Frenk, C. S., White, S. D. M., et al. 2001, MNRAS, 321, 372

Kirkpatrick, C. C., & McNamara, B. R. 2015, MNRAS, 452, 4361

Kravtsov, A. V., & Borgani, S. 2012, ARA&A, 50, 353

Liu, A., Bulbul, E., Ghirardini, V., et al. 2022, A&A, 661, A2

Liu, H., Fabian, A. C., & Pinto, C. 2020, MNRAS, 497, 1256

Lovisari, L., & Reiprich, T. H. 2019, MNRAS, 483, 540

Mantz, A. B., Morris, R. G., Allen, S. W., et al. 2022, MNRAS, 510, 131

McDonald, M., Gaspari, M., McNamara, B. R., & Tremblay, G. R. 2018, ApJ, 858, 45

Mernier, F., & Biffi, V. 2022, arXiv e-prints, arXiv:2202.07097

Mernier, F., de Plaa, J., Kaastra, J. S., et al. 2017, A&A, 603, A80

Mernier, F., Biffi, V., Yamaguchi, H., et al. 2018, SSRv, 214, 129

Mitchell, R. J., Culhane, J. L., Davison, P. J. N., & Ives, J. C. 1976, MNRAS, 175, 29P

Miyazaki, S., Komiyama, Y., Kawanomoto, S., et al. 2018, PASJ, 70, S1

Naab, T., & Ostriker, J. P. 2017, ARA&A, 55, 59

Oguri, M., Miyazaki, S., Li, X., et al. 2021, PASJ, 73, 817

Olivares, V., Salome, P., Combes, F., et al. 2019, A&A, 631, A22

Panagoulia, E. K., Fabian, A. C., & Sanders, J. S. 2014, MNRAS, 438, 2341

Patej, A., & Loeb, A. 2015, ApJL, 798, L20

Pillepich, A., Reiprich, T. H., Porciani, C., Borm, K., & Merloni, A. 2018, MNRAS, 481, 613

Planck Collaboration, Ade, P. A. R., Aghanim, N., et al. 2016, A&A, 594, A24

Planck Collaboration, Aghanim, N., Akrami, Y., et al. 2020, A&A, 641, A6

Press, W. H., & Schechter, P. 1974, ApJ, 187, 425

Rafferty, D. A., McNamara, B. R., Nulsen, P. E. J., & Wise, M. W. 2006, ApJ, 652, 216

Rasia, E., Borgani, S., Murante, G., et al. 2015, ApJL, 813, L17

Reiprich, T. H., Basu, K., Ettori, S., et al. 2013, SSRv, 177, 195

Rossetti, M., & Molendi, S. 2010, A&A, 510, A83

Russell, H. R., McNamara, B. R., Fabian, A. C., et al. 2019, MNRAS, 490, 3025

Sanders, J. S., Fabian, A. C., Russell, H. R., Walker, S. A., & Blundell, K. M. 2016, MNRAS, 460, 1898

Schaye, J., Crain, R. A., Bower, R. G., et al. 2015, MNRAS, 446, 521

Schindler, S., & Diaferio, A. 2008, SSRv, 134, 363

Simionescu, A., Werner, N., Mantz, A., Allen, S. W., & Urban, O. 2017, MNRAS, 469, 1476

Simionescu, A., Allen, S. W., Mantz, A., et al. 2011, Science, 331, 1576

Simionescu, A., ZuHone, J., Zhuravleva, I., et al. 2019, SSRv, 215, 24

Springel, V., White, S. D. M., Jenkins, A., et al. 2005, Nature, 435, 629

Tinker, J., Kravtsov, A. V., Klypin, A., et al. 2008, ApJ, 688, 709

Urban, O., Werner, N., Allen, S. W., Simionescu, A., & Mantz, A. 2017, MNRAS, 470, 4583

Vazza, F., Eckert, D., Simionescu, A., Brüggen, M., & Ettori, S. 2013, MNRAS, 429, 799

Vikhlinin, A., Burenin, R. A., Ebeling, H., et al. 2009, ApJ, 692, 1033

Vogelsberger, M., Genel, S., Springel, V., et al. 2014, MNRAS, 444, 1518

Wang, L., Dutton, A. A., Stinson, G. S., et al. 2017, MNRAS, 466, 4858

—. 2015, MNRAS, 454, 83

Watson, W. A., Iliev, I. T., D'Aloisio, A., et al. 2013, MNRAS, 433, 1230

Zhang, Y.-N., Li, C., Xu, D., & Cui, W. 2022, Experimental Astronomy, 53, 1053

Zhu, Z., Xu, H., Hu, D., et al. 2021, ApJ, 908, 17

Zhuravleva, I., Churazov, E., Schekochihin, A. A., et al. 2014, Nature, 515, 85